Available online at www.sciencedirect.com
SCIENCE DIRECT®
Journal of Nuclear Materials 337–339 (2005) 410–414
journal of nuclear materials
www.elsevier.com/locate/jnucmat

# Kinetic neutral transport effects in the pedestal of H-mode discharges in the DIII-D tokamak ☆

L.W. Owen [a,*], R.J. Groebner [b], M.A. Mahdavi [b]

[a] Oak Ridge National Laboratory, Building 5700, MS-6169, Oak Ridge, TN 37831-8072, USA
[b] General Atomics, P.O. Box 85608, San Diego, CA 92186-9784, USA

**Abstract**

A series of hydrogen and deuterium discharges are analyzed with fluid plasma and Monte Carlo neutrals codes. Comparison of poloidally averaged radial distributions of core neutral density and ionization with analytic solutions of 1-D plasma and neutrals continuity equations support the hypothesis that the width of the density pedestal is largely determined by the neutral source. The increased neutral penetration depth that arises from multiple charge exchange can be included in the analytic model with radially dependent scale lengths. The scale length in the analytic model depends on the neutral fluid velocity which increases across the divertor and pedestal as the neutral atoms charge exchange with the higher temperature background ions. The neutral penetration depth and corresponding density pedestal width depend sensitively on the neutral temperature and the degree of ion-neutral temperature equilibration.


*PACS:* 52.65.y; 52.65.Py; 52.55.Fa; 52.55.Ya
*Keywords:* DIII-D; B2.5-DEGAS; Edge modeling; Neutral transport; Edge pedestal

## 1. Introduction

Understanding the physics that controls the widths of the energy and particle barriers in the H-mode pedestal is necessary in the development of a predictive capability for core confinement in present and future tokamaks. Results from various models [1–3] suggest that the H-mode particle barrier is produced by the combined effects of the edge transport and particle source profiles.

The role of neutrals in H-mode pedestal formation has been addressed in Ref. [4], where a 1-D (radial) analytic model derived [5] from coupled continuity equations for the electron and neutral species densities is shown to be consistent with many features of edge electron density profiles in DIII-D. The model, an extension of the Engelhardt–Fenenberg analytic model [6], shows that the edge density profile results from a self-consistent solution of the particle transport and fueling processes. The observed relationships of pedestal width and height are reproduced for a large number of discharges. The focus of the work reported here is on (1) issues that affect the pedestal particle source but require a numerical treatment and (2) possible modifications to the analytic model that permit the approximate inclusion of these results, thereby extending the region of applicability of the

☆ Work supported by the US DOE under Contracts DE-AC05-00OR22725 and DE-AC03-99ER54463.
* Corresponding author. Tel.: +1 865 574 0634; fax: +1 865 574 1191.
*E-mail address:* owenlw@ornl.gov (L.W. Owen).

0022-3115/$ - see front matter © 2004 Elsevier B.V. All rights reserved.
doi:10.1016/j.jnucmat.2004.10.033

model. These issues include the effects of multiple charge exchange and wall reflections, incomplete ion-neutral temperature equilibration, and 2-D neutrals distributions.

At the present time the only practical way to obtain multidimensional neutrals distributions in the pedestal region is with data-constrained discharge modeling. The analysis technique that is used to reconstruct the plasma is discussed in [7,8] and will be only briefly outlined here. Typically available DIII-D diagnostic data that are used to constrain the model are upstream electron density and temperature profiles from Thomson scattering, divertor and midplane $D_\alpha$ emissivities from filterscope arrays, ion temperature from charge-exchange recombination (CER) spectroscopy, density, temperature and ion flux at the divertor plates from embedded Langmuir probes, $n_e$ and $T_e$ from divertor Thomson scattering, and 2-D radiation profiles. The plasma data are fitted with 2-D stand-alone plasma fluid simulations using the transport code B2.5 [9], and the resulting plasma parameters are used in the Monte Carlo neutrals transport code DEGAS [10] to calculate core fueling rates and neutrals distributions. In the procedure used here the plasma and neutrals codes are not coupled, but satisfaction of the core particle balance equation is imposed as a necessary constraint to ensure consistency of the core fueling rate and the core ion efflux. Iteration of the B2.5 and DEGAS simulations is required in order to simultaneously satisfy the core particle balance and to fit both the plasma and neutrals data.

## 2. Discharge modeling

A total of six H-mode discharges were analyzed at times between ELMs. Four of the discharges used deuterium as the working gas and two used hydrogen. All were lower single null with the ion grad $B$ drift toward the $X$-point. The parameters for each discharge are shown in Table 1. The discharge 110223 is included in order to see effects of larger triangularity.

The two hydrogen discharges differ primarily in the line-averaged density. The deuterium discharges span a range of densities from $4.7\times10^{19}$ to $8.0\times10^{19}\,\mathrm{m}^{-3}$, and input powers from 4.45 to 9.76 MW. The transport coefficients used in the B2.5 analyses are given in Table 1. The heat diffusivities $\chi_i$ and $\chi_e$ are spatially constant and the particle diffusivities $D_\perp$ are composed of a constant term and a term that varies inversely with plasma density (radially increasing). A spatially constant radially outward convective velocity is also used. A positive convective term permits stand-alone deep grid plasma simulations [7] and accounts in an average way for the presence of intermittant plasma objects. The plasma simulations are performed on grids for which the normalized flux $\Psi_N = 0.85$ on the inner core boundary

Table 1
Discharge parameters, transport coefficients, plasma-neutrals analysis results and (constant) density pedestal widths from tanh fitting at the outboard midplane

| Discharge number | 110169 | 110170 | 110223 | 111296 | 110192 | 110194 |
|---|---|---|---|---|---|---|
| Hydrogen isotope (H or D) | D | D | D | D | H | H |
| Density ($10^{19}$ m$^{-3}$) | 4.7 | 7.2 | 7.2 | 8.0 | 4.7 | 3.7 |
| Input power NBI/Ohmic | 4.0/.45 | 4.1/.52 | 8.0/.25 | 9.5/.26 | 3.1/.33 | 3.1/.32 |
| ELM frequency (s$^{-1}$) | 40 | 45 | 70 | 155 | 100 | 85 |
| Radiation – Total/core (MW) | 1.2/.31 | 1.9/.31 | 4.0/.68 | 3.7/.26 | .69/.27 | .59/.23 |
| Stored energy (MJ) | 0.80 | 0.82 | 1.45 | 1.14 | 0.35 | 0.30 |
| Energy confinement time $\tau^E$ (s) | 0.192 | 0.192 | 0.191 | 0.120 | 0.113 | 0.094 |
| Lower triangularity | 0.191 | 0.251 | 0.432 | 0.239 | 0.176 | 0.175 |
| B2.5 particle conf. time $\tau^p$ (s) | 0.146 | 0.161 | 0.105 | 0.194 | 0.082 | 0.081 |
| B2.5 Inner plate current (A) | 2025 | 5663 | 4764 | 8108 | 3062 | 2240 |
| B2.5 Outer plate current (A) | 3159 | 4880 | 4332 | 5855 | 4259 | 3290 |
| B2.5 Core efflux (A) | 993 | 1347 | 1995 | 1239 | 1707 | 1364 |
| DEGAS core fueling rate (A) | 939 | 1288 | 1947 | 1079 | 1635 | 1316 |
| NBI fueling rate (A) | 77 | 78.2 | 154 | 183 | 59.7 | 59.1 |
| Power across sep. (Exp) (MW) | 4.14 | 4.27 | 7.57 | 9.50 | 3.11 | 3.18 |
| Power across sep. B2.5 (MW) | 3.89 | 4.19 | 8.87 | 9.32 | 3.15 | 3.02 |
| B2.5 $D_\perp$ – const. term (m$^2$/s) | 0.002 | 0.006 | 0.003 | 0.001 | 0.030 | 0.030 |
| B2.5 $D_\perp$ – term $\propto 10^{20}$ (m$^3$/s)/$n$ | 0.006 | 0.006 | 0.012 | 0.003 | 0.003 | 0.005 |
| Convective velocity (m/s) | 1.50 | 2.35 | 3.80 | 2.30 | 5.00 | 4.50 |
| B2.5 $\chi_i$ (m$^2$/s) | 0.33 | 0.30 | 0.50 | 0.78 | 0.50 | 0.55 |
| B2.5 $\chi_e$ (m$^2$/s) | 0.33 | 0.30 | 0.20 | 0.78 | 0.50 | 0.55 |
| Flux expansion rel. to midplane | 7.47 | 7.30 | 5.79 | 5.78 | 7.65 | 7.13 |
| $\Delta_e$ (constant) from tanh fit (cm) | 1.75 | 1.29 | 1.12 | 0.835 | 1.52 | 1.65 |

in order to define the poloidally averaged neutrals quantities more deeply into the core plasma.

With the exception of the divertor and midplane $D_\alpha$ intensities, which are computed with DEGAS, all of the diagnostic data discussed above are compared to results of stand-alone plasma simulations. In general the quality of the fits to the discharge data is comparable to that shown in Refs. [7,8]. The B2.5 code uses an internal neutrals model [11] that has been benchmarked against DEGAS, rather than being linked with the Monte Carlo code itself. As discussed above, in order to ensure global consistency of the plasma and neutrals simulations, the B2.5 and DEGAS calculations are iterated until the core fueling rate, from divertor recycling (DEGAS) and neutral beams, is consistent with the core plasma particle efflux calculated with B2.5. These quantities are compared in Table 1 for each of the discharges analyzed.

## 3. Poloidally averaged distributions – comparisons with 1-D model

Since core fueling in these discharges is dominated by divertor recycling, the neutrals distributions in the confined plasma are intrinsically 2-D. In Fig. 1 the poloidal distribution of ion source rate just inside the separatrix shows that fueling across the $X$-point dominates upstream fueling arising from divertor leakage. To facilitate comparison of the fueling depth in different discharges, radial distributions in the core plasma are generated by forming poloidal averages in the following way. With $r$ the reference radial coordinate and $\theta$ the poloidal coordinate,

$$S_i(r) = \int_0^{2\pi} d\theta s_i(r,\theta) n_0(r,\theta) \Big/ \int_0^{2\pi} d\theta n_0(r,\theta), \quad (1)$$

where $s_i(r,\theta)$ is the ionization rate in the grid cell centered at $(r,\theta)$.

In the 1-D analytic model [4,5], the radial profiles of electron and neutral atom densities are of the forms

$$n_e(z) = A_e \tanh\{C + z/(2\Delta)\} + B_e \quad (2)$$

and

$$n_0(z) = A_0 \sec h^2(C + z/\Delta) + B_0, \quad (3)$$

where $\Delta$ is the neutral penetration length and the radius-like variable $z = (r_{sep} - r)$ is positive in the core plasma. Eqs. (2) and (3) are written in the form used for fitting, with $A_{e,0}$, $B_{e,0}$, and $\Delta$ the fit parameters. The form of Eq. (2) required to fit DIII-D L-mode profiles and H-mode profiles to the center of the plasma is the modified tanh function, in which the $\exp(+z/\Delta)$ term in the numerator of the tanh function is multiplied by a factor $(1 + \alpha z)$. A fit to just the pedestal region often does not require the modified form of the tanh function in H-mode; this is the case for the discharges analyzed here.

Constant values of $\Delta$ that reproduce $n_e(z)$ in the pedestal region are given in the last line of Table 1. With these (constant) values of $\Delta$ two functional forms are used to compare with $n_0(z)$ calculated with DEGAS. The first, given by Eq. (3), fits the $n_0$ profile near the separatrix but decays more rapidly into the plasma than the DEGAS result. The second form, an exponential, fits only in an average sense. Why does constant $\Delta$ fit the $n_e$ profile but not that of $n_0$? One possibility is that the $n_0$ scale length, which is proportional to the neutral velocity $V_0$ [5], can vary strongly with $z$ as the neutrals charge exchange with the hotter background ions. $V_0$ should vary at least as fast as $T_0^{1/2}$. In Fig. 2 are shown the ion and neutral atom temperature profiles in the SOL and core regions for the H and D discharges 110192 and 110169, respectively. In neither of the discharges do the ions and atoms equilibrate at the separatrix or in the pedestal region. However in both cases it is seen that $d\ln T_0/dz \approx d\ln T_i/dz$. Since the neutrals leave the divertor as two energy groups, Franck Condon atoms and energetic reflected atoms, at moderate density they are not expected to have a Maxwellian distribution in the SOL or pedestal region near the separatrix. The possibly non-Maxwellian neutrals distribution and the dependence of the charge-exchange reaction rates on the neutral particle energy can lead to $V_0$ varying even more strongly with $z$ than does $T_0^{1/2}$.

It is noted in Table 1 that the $n_e$ scale length for the deuterium discharge is larger than that for hydrogen,

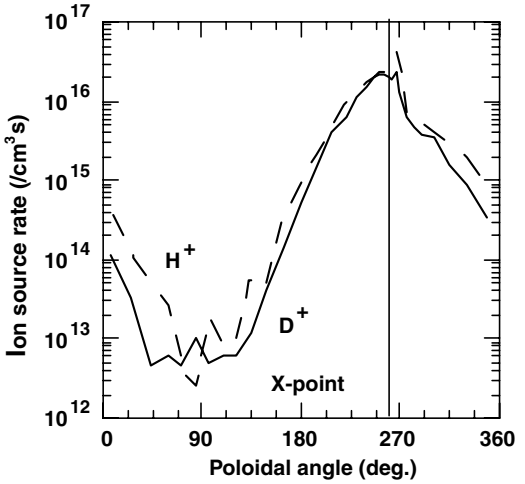


Fig. 1. The poloidal distribution of the ion source rate just inside the separatrix shows little dependence upon the isotope mass for the equal density H and D discharges 110192 and 110169. This is primarily due to the 1/3 larger input power in 110169 which results in higher $T(D^0)$ in the divertor and pedestal region and comparable neutral mean-free paths in the plasma.

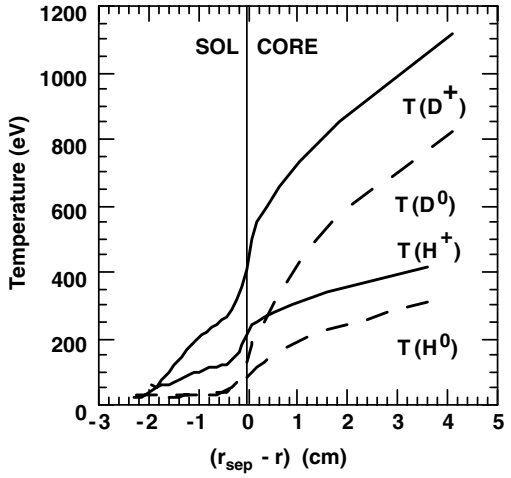


Fig. 2. Deuterium and hydrogen atom and ion temperatures in the SOL and pedestal regions (from DEGAS and Thomson scattering, respectively) show that the neutrals have not completely equilibrated with the ions in discharges 110169 and 110192. These results also show the strong spatial dependence of the neutral atom temperature and a corresponding need for spatial dependence in the neutral fluid velocity and corresponding penetration length.

even though one expects the less massive H atoms to have a larger penetration depth. The reason for this is seen in Fig. 2, where due to larger input power, $T(D^0)$ is almost a factor of three larger than $T(H^0)$.

Based on the inadequacy of constant $\Delta$ to describe the $n_0$ profile from Monte Carlo, a spatial dependence of the form $\Delta(z) = a + bz^{\gamma}$, where $a$, $b$, and $\gamma$ are fit parameters, is investigated and shown in Fig. 3 to simultaneously fit both profiles. Moreover the fits are achieved with the $n_e$ scale length equal to the $n_0$ value, as in the 1-D analytic model [12]. For the discharges analyzed here the power $\gamma$ is almost constant, with values between 0.7 and 0.75. Likewise the values of $a$ and $b$ vary by only a few percent from their median values of 0.22 and 0.50, respectively.

## 4. Conclusions

The relationship of the neutral penetration length and the width of the H-mode density pedestal has been investigated by plasma reconstruction using detailed data-constrained discharge modeling with stand-alone fluid plasma and Monte Carlo neutrals transport codes. Poloidally averaged radial neutrals distributions are compared to a 1-D analytic model, the solution of which has been widely used to fit DIII-D electron density profiles from Thomson scattering. It is found that the model can fit both the Thomson $n_e$ profile and the corresponding $n_0$ profile from Monte Carlo if the neutral penetration length $\Delta$ is a function of the radial coordinate. This indicates a strong correlation of the width of the H-mode density pedestal and the neutral penetration length. The origin of the spatial dependence of $\Delta$ is in the proportionality of $\Delta$ to the neutral fluid velocity, which increases when the neutrals undergo charge exchange with the hotter background ions as they traverse the SOL and pedestal. In general the neutral scale length in the pedestal is sensitive to both the plasma density and temperature (or input power). For example, $\Delta$ for a deuterium discharge with the same density as one in hydrogen, but with 1/3 larger input power, was found to be larger than the hydrogen value because of higher ion temperature.

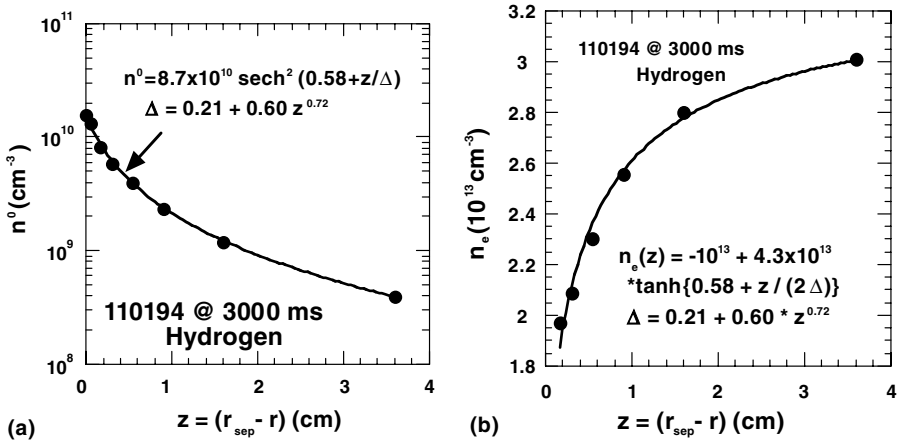


Fig. 3. The incorporation of spatial dependence in the neutral penetration length $\Delta$ is seen to enable simultaneous fitting of the neutral atom (a) and electron (b) densities in the pedestal region. The spatial dependence of $\Delta$ is slightly stronger than that of $T_0^{1/2}$ due possibly to non-Maxwellian neutrals and the $E_0$-dependence of $\langle \sigma v \rangle_{cx}$.

## References

[1] A.E. Hubbard, Plasma Phys. Control. Fusion 42 (2000) A15.
[2] F.L. Hinton, G.M. Staebler, Phys. Fluids B 5 (1993) 1281.
[3] V.B. Lebedev, P.H. Diamond, Phys. Plasmas 4 (1997) 1087.
[4] R.J. Groebner, M.A. Mahdavi, A.W. Leonard, et al., Phys. Plasmas 9 (2002) 2134.
[5] M.A. Mahdavi, T.H. Osborne, A.W. Leonard, et al., Nucl. Fusion 42 (2002) 52.
[6] W. Engelhardt, W. Fenenberg, J. Nucl. Mater. 76&77 (1978) 518.
[7] B.A. Carreras, L.W. Owen, R. Maingi, et al., Phys. Plasmas 5 (1998) 2623.
[8] L.W. Owen, R. Maingi, D.K. Lee, et al., J. Nucl. Mater. 220–222 (1995) 315.
[9] B.J. Braams, Contrib. Plasma Phys. 36 (1996) 276.
[10] D.B. Heifetz, D. Post, M. Petravic, et al., J. Comp. Phys. 46 (1982) 309.
[11] R. Maingi, J.T. Hogan, L.W. Owen, et al., Nucl. Fusion 34 (1994) 283.
[12] M.A. Mahdavi, R.J. Groebner, A.W. Leonard, et al., Bull. Am. Phys. Soc. 47 (2002) 227.